



## Acoustic measurements of the spatial and temporal structure of the near-bottom boundary layer in the 1990–1991 STRESS experiment

JAMES F. LYNCH,\* JAMES D. IRISH,\* THOMAS F. GROSS,†  
PATRICIA L. WIBERG,‡ ARTHUR E. NEWHALL,\* PETER A.  
TRAYKOVSKI§ and JOSEPH D. WARREN§

(Received 28 December 1994; in revised form 16 January 1996; accepted 16 December 1996)

**Abstract**—As part of the 1990–1991 Sediment TRansport Events on Shelves and Slopes (STRESS) experiment, a 5 MHz Acoustic BackScatter System (ABSS) was deployed in 90 m of water to measure vertical profiles of near-bottom suspended sediment concentration. By looking at the vertical profile of concentration from 0 to 50 cm above bottom (cmab) with 1 cm vertical resolution, the ABSS was able to examine the detailed structure of the bottom boundary layer created by combined wave and current stresses. The acoustic profiles clearly showed the wave–current boundary layer, which extends to (order) 10 cmab. The profiles also showed evidence of an “intermediate” boundary layer, also influenced by combined wave and current stresses, just above the wave–current boundary layer. This paper examines the boundary-layer structure by comparing acoustic data obtained by the authors to a 1-D eddy viscosity model formulation. Specifically, these data are compared to a simple extension of the Grant-Glenn-Madsen model formulation. Also of interest is the appearance of apparently 3-D “advective plume” structures in these data. This is an interesting feature in a site which was initially chosen to be a good example of (temporally averaged) 1-D bottom boundary-layer dynamics. Computer modeling and sector-scanning sonar images are presented to justify the plausibility of observing 3-D structure at the STRESS site. © 1997 Elsevier Science Ltd

### 1. INTRODUCTION

In this paper the authors examine a typical mid-depth continental shelf bottom boundary layer (BBL) in which a combination of waves and currents provides the bottom stress, and currents provide the net transport. Of particular interest are the details of the time-averaged 1-D vertical structure of the boundary layer and time-dependent 3-D advective effects. A trio of intensive field experiments collectively called “STRESS” (Sediment TRansport Events on Shelves and Slopes) has been performed off the northern California coast during the years 1988–1989, 1990–1991 and 1994–1995 (see Fig. 1) to study the BBL (Trowbridge and Nowell, 1994). This paper concentrates on measurements made by an acoustic sediment concentration profiling instrument called “ABSS” (Acoustic BackScatter System) deployed in STRESS during the 1990–1991 field exercise (Lynch *et al.*, 1994) which showed details of

---

\* Woods Hole Oceanographic Institution, Woods Hole, MA 02543-1053, U.S.A.

† Skidaway Institute of Oceanography, 10 Ocean Science Circle, Savannah, GA 31411, U.S.A.

‡ Department of Environmental Sciences, University of Virginia, Charlottesville, VA 22903, U.S.A.

§ MIT/WHOI Joint Program in Oceanography and Oceanographic Engineering, Woods Hole, MA 02543, U.S.A.

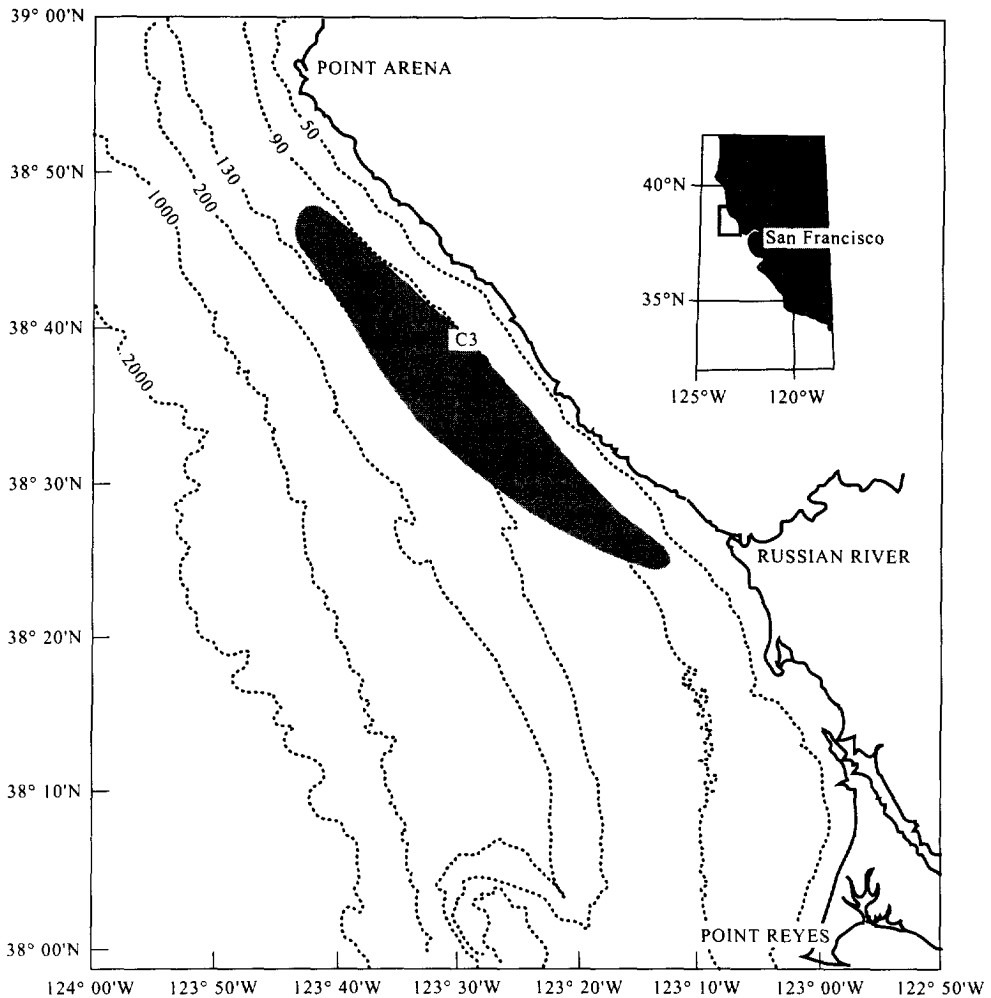


Fig. 1. Site location for the 1990–1991 STRESS experiment. The ABSS instrument was deployed at the mid-shelf C3 site in 90 m of water. “Mud belt” region is the dark, shaded area.

the near bottom boundary-layer structure. The 1995 measurements of the bottom roughness made with a sector scanning sonar and a stereo survey camera will also be considered.

This paper is organized as follows: following this introduction, in Section 2 the background of the STRESS experiment is discussed and the measurements made during it, most particularly the ABSS measurements. In Section 3 the nature of the boundary layer at the STRESS site is discussed and how it might be modeled. Section 4 covers the ABSS observations of the 1-D vertical structure of the boundary layer, with the emphasis being on observations of an “intermediate boundary layer” between the wave and current boundary layers. Section 5 discusses the instantaneous 3-D nature of the boundary layer inferred from the ABSS observations, computer modeling and rotary sector scanning sonar images of the bottom. Section 6 presents a discussion and conclusions.

## 2. THE STRESS EXPERIMENT AND THE ABSS INSTRUMENT

The STRESS experiment was a large, multi-year experiment designed to examine the scientific issues involved in sediment transport in the region of the continental shelf outside of the surf zone, but still shallow enough that surface gravity waves interact with the bottom. Of particular interest in STRESS were the long period waves produced by large winter storms in the Pacific — these are particularly effective in suspending sediment and making it available for transport (Sherwood *et al.*, 1994). To measure the physical quantities needed to describe the BBL and sediment transport, a large number of autonomous instruments were deployed on several tripods at the STRESS site. These included BASS (Benthic Acoustic Stress Sensor) current meters to measure the vertical structure of horizontal current (Williams *et al.*, 1987); a stereocamera to measure the bottom microtopography (Wheatcroft, 1994); pressure sensors to measure the wave field; and OBSs (Optical Backscattering Sensors), the ABSS, and transmissometers to measure the vertical profile of suspended sediment concentration (Lynch *et al.*, 1994). Many other instruments were also deployed (e.g. Sherwood *et al.*, 1994), but the above ones are the most germane to the present discussion.

### 2.1. ABSS characteristics

The ABSS instrument was deployed at the 90 m mid-shelf site in all three STRESS deployments. This instrument actually consists of two backscattering sonars: a downward looking one at 5 MHz which profiles over 128 cm with 1 cm vertical resolution, and an upward looking one at 1 MHz which profiles over 26 m with 20 cm vertical resolution (see Fig. 2). This paper considers the 5 MHz measurements, as the primary concern will be the lower portion of the BBL. Due to transducer placement, and the rejection of near-transducer data due to ringing effects, only the data from the lower 50 cm of the water column are utilized.

The ABSS system sampled a 106-second period at 2 Hz every half hour and the results were recorded on a 60 MByte internal tape drive with a capacity for about 3 months of data. Each 106-second burst was composed of 53 “average pings” which were internal averages of four “real pings” made over 2 s at a 2 Hz rate. Of these 53 profiles on tape, the first 12 were made at a low-power output, the next 40 were made at high-power output and the last profile was made with no transmitted power, to be used as an estimate of the system noise level. These 53 sample bursts allow the data to be analyzed in two modes: (i) a slow schedule produced by averaging the 40 high-power profiles together to get a sample for each half-hour interval; and (ii) a high frequency or fast sampling mode where each of the 2-s average profiles in a burst is analyzed to resolve any events associated with surface wave frequencies.

The sampling scheme noted above was chosen not only to deal with temporal sampling issues, i.e. to prevent aliasing at the frequencies of the physical processes monitored, but also with Rayleigh amplitude statistics in mind, i.e. the noisiness (variance) in the data one sees due to the random phase interference in the backscattering from individual particles. If each ping sent out sees a completely independent realization of the sediment in the boundary layer, which (in the most conservative estimation, ignoring particle reconfiguration by turbulence) it will if the wave and/or current speed is at least 5 cm in the 0.5-second sample interval, or roughly  $10 \text{ cm s}^{-1}$ , then the backscatter standard deviation of the amplitude is  $1/\sqrt{N}$ , where  $N$  is the number of pings averaged. (The measured standard deviation is

# Acoustic Backscatter System ABSS

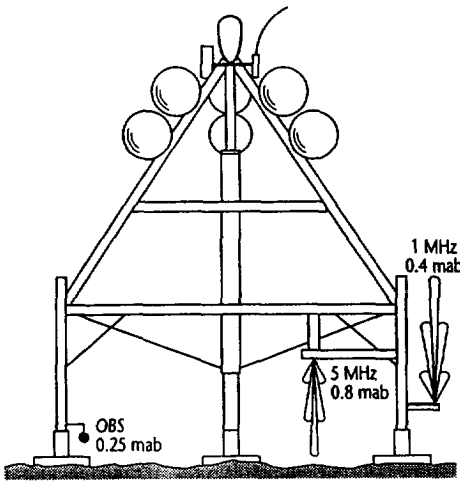


Fig. 2. Instrumental characteristics of the ABSS as deployed in the 1990–1991 STRESS experiment.

## Upward Looking System

Frequency: 1 MHz  
 Beam Width:  $\sim 0.8^\circ$  (3db)  
 Pulse Width: 260  $\mu\text{sec}$   
 Range Increments: 0.2 meter  
 Averaging Time: 0.26 msec  
 Detector: Full Wave (absolute value)  
 Digitizer Dynamic Range: 12 bits (1:4096)  
 Recorder Capacity: >6000 profiles  
 No. of Range Increments: 127

## Downward Looking System

Frequency: 5 MHz  
 Beam Width:  $\sim 0.8^\circ$   
 Pulse Width: 10–12  $\mu\text{sec}$   
 Range Increments: 1 cm  
 Averaging Time: 12  $\mu\text{sec}$   
 Detector: Full Wave (absolute value)  
 Digitizer Dynamic Range: 12 bits  
 Recorder Capacity: >6000 profiles  
 No. of Range Increments: 127

## General

Sample Rate: 1 profile / 10 sec (fastest)  
 to 1 profile / 6 hrs (slowest)  
 Battery Life: 120+ Days  
 Depth Capacity: 6000 meters

actually less due to the 0.26 ms temporal averaging of each ping produced by the instrument.) Four pings resulted in approximately a 25% standard deviation in the observed acoustic pressure magnitude,  $|p|$ . By averaging 40 pings in the slow sampling, the deviation in  $|p|$  is cut to about 14%. The particle concentration, which is the desired number, is directly proportional to the acoustic intensity,  $|p|^2$ , so that the concentration estimates show a 30% error for slow sampling and a 50% error for fast sampling.

## 2.2. Vertical concentration profile estimation using ABSS

An important output from the ABSS is the estimate of the vertical concentration profile. This quantity is estimated from the raw acoustic profile data, i.e. the backscattered pressure amplitude,  $|p(z)|$ , vs distance  $z$  from the transducer. To calculate relative concentrations from such backscattering amplitude data, we first compute the “system response function”,

$R(z)$ , from the active sonar equation. The procedure for this has been discussed at length in the literature (Hay, 1983; Lynch, 1985) and so will not be pursued extensively here.  $R(z)$  gives the response of the system to a spatially uniform concentration, size distribution and material composition of suspended sediments (assumptions which are discussed in more detail later in this paper). The sonar equation used to calculate  $R(z)$  includes parameters for: (1) spreading loss; (2) medium attenuation, which is primarily due to water molecule relaxation effects and scattering by the particulates themselves; and (3) the nearfield beam pattern of the transducer. The latter effect is normally not important except near the transducer. Several of these parameters are determined from experimental calibration data. Having calculated  $R(z)$ , the noise power was then subtracted from the total intensity return (using the 53rd average ping or “noise ping” where no signal was transmitted in order to estimate the noise power) to obtain  $|p_{\text{signal}}|^2$  and  $|p_{\text{signal}}|^2$  was then divided by  $R^2(z)$  to obtain the (relative) concentration.

One property of the ABSS instrument which is of particular importance to this study is its preferential, almost “tuned” response to the larger particles in suspension. Figure 3 shows a plot of instrument response times, the volume fraction distribution of particle sizes measured by Wheatcroft and Butman (1997) at the mid-shelf STRESS site in area preserving form. This figure shows the response of the 1 MHz and 5 MHz ABSS instruments and the OBS. The optical device’s response to the STRESS sediment sizes ( $\times a$  for the area preserving form), reflects the particle size distribution itself; this also shows the well known geometrical optics response to a particle’s cross-sectional area, not its volume. The 1 and 5 MHz acoustics, however, have mostly a “volume squared” scattering law for the STRESS sediments, leading to a strong preference for the larger particulates seen. Specifically, the 5 MHz acoustics respond most strongly to 50  $\mu\text{m}$  diameter sediments; later in this paper the rough approximation that the ABSS response is “tuned” to this size is made. This is not strictly true and for the reader interested in a more exact account of how acoustics devices respond to particle size for the type of continental shelf sediments encountered at the STRESS site, we refer to Lynch *et al.* (1994).

### 3. STRUCTURE OF THE BOTTOM BOUNDARY LAYER — (1-D MODELS, 3-D EFFECTS AND TEMPORAL STRUCTURE)

This section briefly reviews some of the concepts of the nature of the bottom boundary layer which have evolved, particularly in the context of eddy viscosity formulations. The section mainly concentrates on 1-D (time-independent) modeling of the boundary layer, though not exclusively, as 3-D and time-dependent effects are also of relevance to this site.

The interest here is in BBLs that are produced by a combination of wave and current induced bottom stresses on the continental shelf. A great deal of work on modeling such boundary layers was performed by O. Madsen, W. Grant, and S. Glenn (among many others) during the late 1970s and early 1980s. The analytical/numerical model of the BBL which was produced by their particular work is commonly called the “GGM model” (Grant and Madsen, 1979; Grant and Madsen, 1986; Glenn and Grant, 1987); it is a time-independent 1-D eddy viscosity model which takes wave, current and bottom property (mainly roughness) information as inputs and produces from these the vertical profile of turbulence, the bottom roughness evolution, the suspended sediment concentration, and other quantities of interest. Due to the differing time scales of the waves and currents, the bottom boundary layer breaks into two boundary layers, the so-called wave–current and

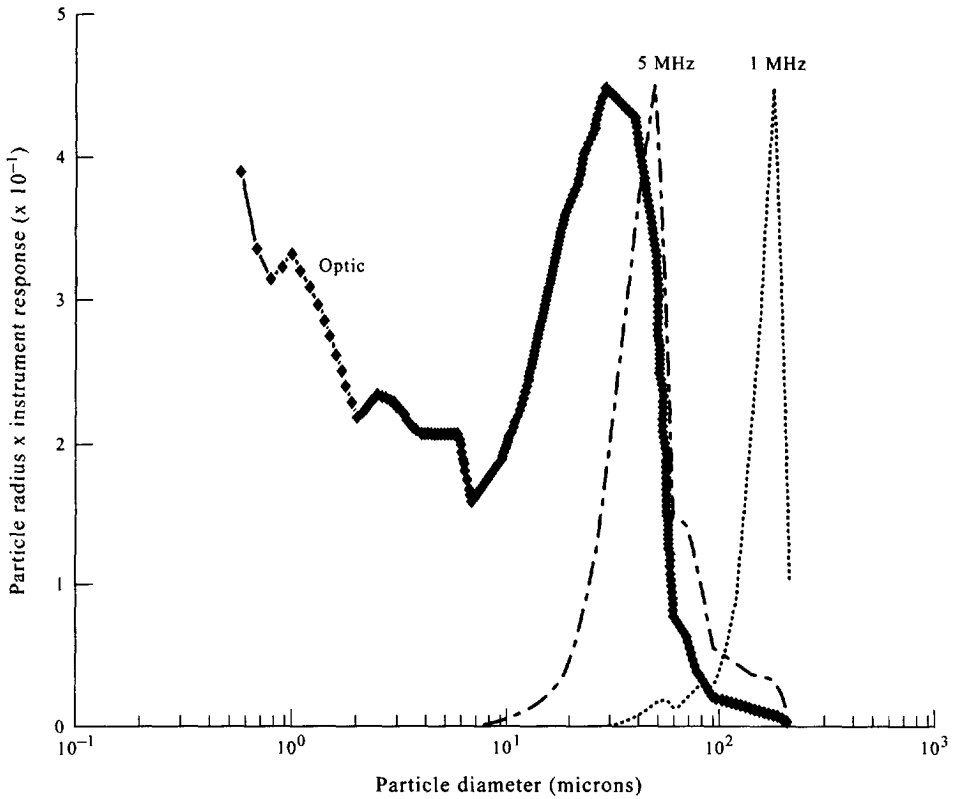


Fig. 3. Particle radius  $\times$  instrument response to STRESS site sediments for optical instruments (e.g. OBS, transmissometer), the 5 MHz ABSS instrument, and the 1 MHz ABSS instrument. Optic's response to the cross-sectional area of the particles  $\times$  an additional factor of  $a$  reproduces the particle size spectrum at the STRESS site. The "tuning" of the 5 MHz ABSS system to the 50  $\mu\text{m}$  diameter sediments is also seen clearly. Factor of  $a$  was used to preserve the area under the logarithmic plot.

current boundary layers. The thickness of the wave-current boundary layer is given (roughly) by the relation:

$$\delta_{cw} \approx \frac{\kappa u_*^{cw}}{\omega} \sim 10 \text{ cm} . \quad (1)$$

If the STRESS site was not sloping and was unstratified, the thickness of the current boundary layer would be given by:

$$\delta_c \approx \frac{\kappa u_*^c}{f} \sim 20 \text{ m} . \quad (2)$$

However, work by Lentz and Trowbridge (Lentz and Trowbridge, 1991; Trowbridge and Lentz, 1991) has shown that stratification and cross-shelf advection of buoyancy also influence the BBL height at the STRESS site. Thus, a better estimate of  $\delta_c$  is 10 m for this site.

In equations (1) and (2),  $\delta_{cw}$  and  $\delta_c$  are the wave-current and current boundary-layer

thicknesses, respectively;  $u_*^{cw}$  is a combined (non-linear) wave–current friction velocity which can be calculated by the GGM model;  $u_*^c$  is the current induced friction velocity;  $\omega$  is the dominant (radial) surface gravity wave frequency;  $f$  is the local inertial frequency; and  $\kappa$  is Von Karman’s constant, 0.4. If one makes the approximation of a linear eddy viscosity model, i.e.

$$K = \kappa u_*^{cw} z \quad z \leq \delta_{cw}, \quad (3)$$

$$K = \kappa u_*^c z \quad z > \delta_{cw}, \quad (4)$$

and assumes an equilibrium balance between vertical turbulent diffusion and gravitational settling, then the vertical suspended particulate concentration profile can be written in the simple form (Rouse, 1937):

$$C_n(z) = C_n(z_r(\text{layer})) \left( \frac{z}{z_r(\text{layer})} \right)^{w_n/\kappa u_{\text{layer}}}, \quad (5)$$

where

$$u_{\text{layer}} = \begin{cases} u_*^{cw} & z \leq \delta_{cw} \\ u_*^c & z \geq \delta_{cw} \end{cases}. \quad (6)$$

The concentration in the current–wave layer is based upon a prescribed reference concentration at a height within  $\delta_{cw}$ ,  $C_n(z_r(\text{layer}))$ . The concentration in the upper layer is determined by matching across the transition at  $z = \delta_{cw}$ :

$$C_n(z_r(\text{layer})) \left( \frac{\delta_{cw}}{z_r(\text{layer})} \right)^{-w_n/\kappa u_*^{cw}} = C_n(\delta_{cw}) \left( \frac{\delta_{cw}}{\delta_{cw}} \right)^{-w_n/\kappa u_*^c}. \quad (7)$$

The slope of this simple concentration profile on a log  $C$  vs log  $z$  plot is given by:

$$S = \frac{-w_n}{\kappa u_{\text{layer}}}. \quad (8)$$

In order to have a model of the time invariant eddy viscosity which is continuous with height, Madsen and others have proposed a  $K(z)$  given by Madsen and Wikramanayake (1991):

$$K(z) = \begin{cases} \kappa u_*^{cw} z & z \leq \alpha \delta_{cw} \\ \kappa u_*^{cw} \alpha \delta & \alpha \delta_{cw} \leq z \leq \alpha \delta_{cw} / \varepsilon, \\ \kappa u_*^c z & \alpha \delta_{cw} / \varepsilon \leq z \end{cases}, \quad (9)$$

where  $\alpha$  is the fraction of the wave boundary layer over which the eddy viscosity varies linearly and

$$\varepsilon = \frac{u_*^c}{u_*^{cw}}. \quad (10)$$

Introduction of this model maintains continuous gradients of current speed. In the ABSS data examined later in this paper, it appears that one is seeing wave–current interaction effects that are consistent with  $\alpha = 2$  in equation (9). If  $\ell^{cw} = 2\delta_{cw}$  in equation (9), then this results in the type of picture shown in Fig. 4. The heights of the wave–current boundary

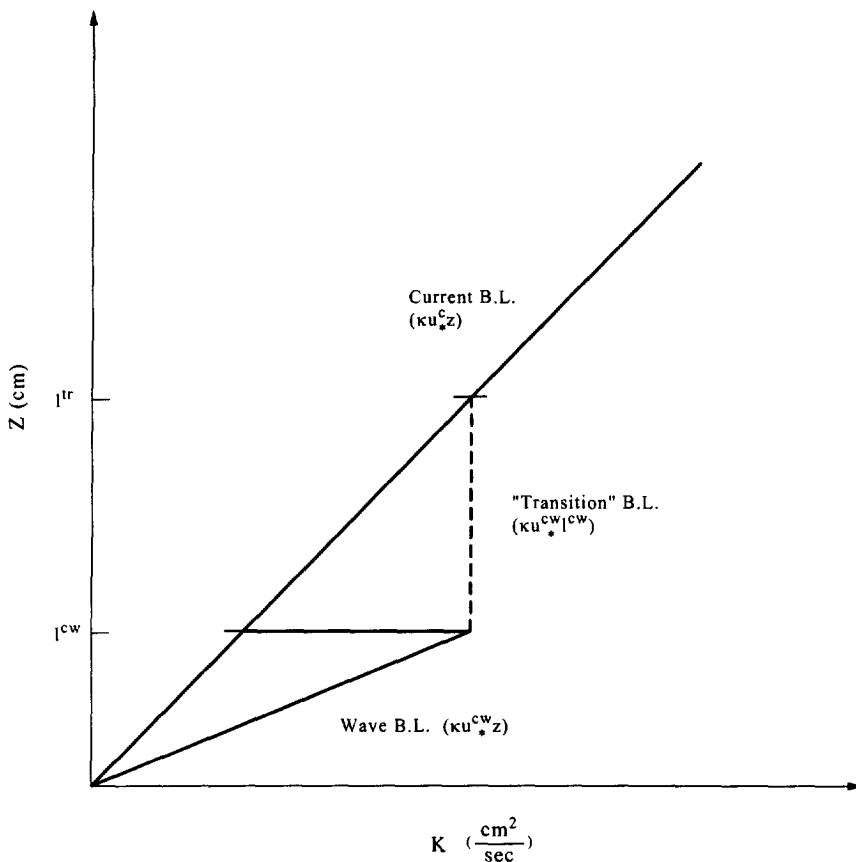


Fig. 4. Eddy viscosity vs height for older and “modified” Grant-Glenn-Madsen (GGM) models. Use of a constant eddy viscosity above the wave-current boundary layer gives a well defined intersection with the current boundary layer.

layer and the “transition layers” are clearly visible features of the model in this figure — it is possible to see later in this paper that this is also true for the ABSS data.

Looking at equation (9), it can be seen that the concentration profile shape for the wave-current and current boundary layers will still be Rouse (log layer), but that the transition region will be an exponential profile, given by:

$$C(z) = C(\ell^{cw}) \exp \left\{ \frac{-w_n}{\kappa u_*^{cw} \ell^{cw}} \cdot (z - \ell^{cw}) \right\} \quad \alpha \delta_{cw} \leq z \leq \frac{\alpha \delta_{cw}}{\epsilon} \quad (11)$$

It will be seen that the acoustic concentration profile measurements are in some ways consistent with this type of transition layer.

A question that needs to be asked each time one uses the GGM model is: is the region of interest really approximately 1-D, i.e. is  $\ell^{CORR} \ll \ell^{WAVE EX}$ , where  $\ell^{CORR}$  is the bottom roughness correlation length and  $\ell^{WAVE EX}$  is the wave excursion length? Previous measurements at the mid-shelf STRESS site (Wheatcroft, 1994) suggest that the  $\ell^{CORR} \approx 10$  cm, while pressure records indicate  $\ell^{WAVE EX} \approx 1-2$  m. Therefore, a 1-D

assumption should have been accurate. However, the ABSS data show some 3-D “plume” effects which would seem to contradict this model condition. A. E. Hay (personal communication, 1994) has suggested that these sediment plumes may be due to nearby large scale roughness elements or scour marks due to the tripod legs, and indeed are 3-D effects.

Originally, it was thought that the 1-D vs 3-D issue was likely not to be determined. However, in 1995 the instruments from the third and final STRESS deployment, made at the same site as the 1990–1991 deployment, were recovered. Among these instruments was an autonomous rotary sector scanning sonar (Hay and Wilson, 1994), which acoustically imaged the bottom microtopography with 1–10 cm resolution over a circle of  $\approx 2$  m radius once an hour for 4 months (October 1994–February 1995). Additionally, the stereocamera which was used by Wheatcroft in 1990–1991 (Wheatcroft, 1994) was again deployed and bottom contact camera surveys were made at deployment and recovery. The images from these instruments clearly showed sizeable biologically produced burrows and mounds (see Fig. 5) which are believed in fact to be strong candidates for the type of 3-D roughness element suggested by A. E. Hay. At almost the same time, T. Gross produced a simple model of plume structure which closely resembled the observed results, based on having discrete point sources of sediment produce 3-D advection. Both the sonar and optical observations and Gross’ plume model will be discussed in more detail in a later part of this paper dealing with 3-D effects.

Given that it is probable that 3-D advection effects are being observed, in addition to turbulent diffusion, exactly what type of model is most appropriate for the STRESS site should be discussed. Three classes of model quickly come to mind: (1) 1-D eddy viscosity models, such as the GGM model already discussed; (2) “advection–diffusion” models (e.g. Nielsen, 1992); and (3) full turbulence closure models (e.g. Fredsoe and Deigaard, 1992). This paper concentrates mainly on 1-D eddy viscosity models, as they are simple to use for “practical” transport calculations. Eddy diffusivity models describe average quantities influenced by turbulent flow fluctuations, but offer little insight into the temporal and spatial structure of those fluctuations. However, such models only make sense for the STRESS site if the instantaneous 3-D advective effects can somehow be averaged spatially or temporally into an “effective 1-D eddy viscosity”, perhaps with a profile like that in the extended GGM model. The second class of model is the so-called “advective–diffusive” model, in which one treats the transport process as partly advective and partly diffusive. In general, diffusive transport is displayed by the finer particles, while the coarse particles are more influenced by convective mechanisms (see, for example, Nielsen, 1992). Such a model seems most consonant with the observations made at the STRESS site. The third class of model is the “turbulence closure” kind, in which one derives the bed shear stresses from transport equations for the kinetic energy and dissipation. These models, while perhaps the most “exact” of the three, are more computationally intensive and are less directly insightful physically. They do, however, automatically include the transition between the wave and current boundary layers in a smooth and consistent fashion. The emphasis in this paper will be on the first two models, particularly the first.

#### 4. VERTICAL STRUCTURE OF THE NEAR-BOTTOM BOUNDARY LAYER AS OBSERVED BY ACOUSTIC BACKSCATTERING MEASUREMENTS

This section examines the structure of the lowest 50 cm of the bottom boundary layer,

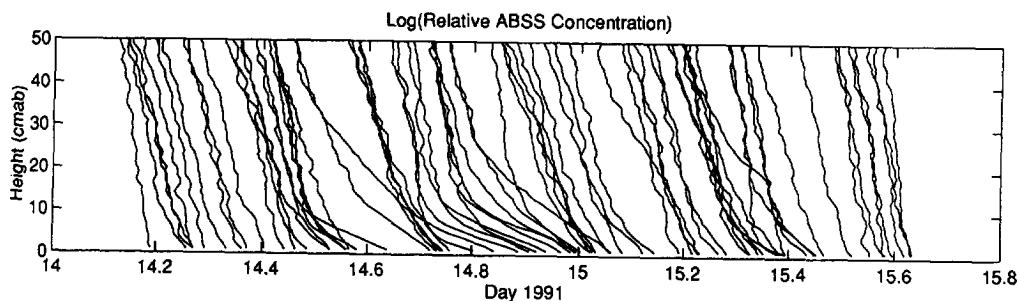


Fig. 6. Plot of  $\log C$  vs  $z$  for 1.6 days of ABSS acoustic data during the 1990–1991 STRESS experiment. Change of profile shape near the top of the wave boundary layer is quite apparent during “storm periods”.

using the acoustic backscatter measurements of concentration provided by ABSS. The first thing to look at is the estimate of  $\ell^{cw}$  provided by distinct changes in the acoustic backscatter slopes. By looking at plots of  $\log C$  vs  $\log z$  and also of  $\log C$  vs  $z$  (which will give straight line slopes for Rouse and exponential concentration profiles, respectively), a distinct, abrupt slope change point at the nominal height of the wave boundary layer was consistently found, generally between 0 and 15 cm above bottom (see Fig. 6). To ascertain that this point was indeed the top of the wave boundary layer, the GGM model was employed, using  $K(z)$  computed from the wave, current, bottom sediment type and roughness measurements taken as part of STRESS. From this model’s output of  $u_*^{cw}$ , an estimate of  $\ell^{cw}$  is obtained from:

$$\ell^{cw} = \frac{2 \kappa u_*^{cw}}{\omega} . \quad (12)$$

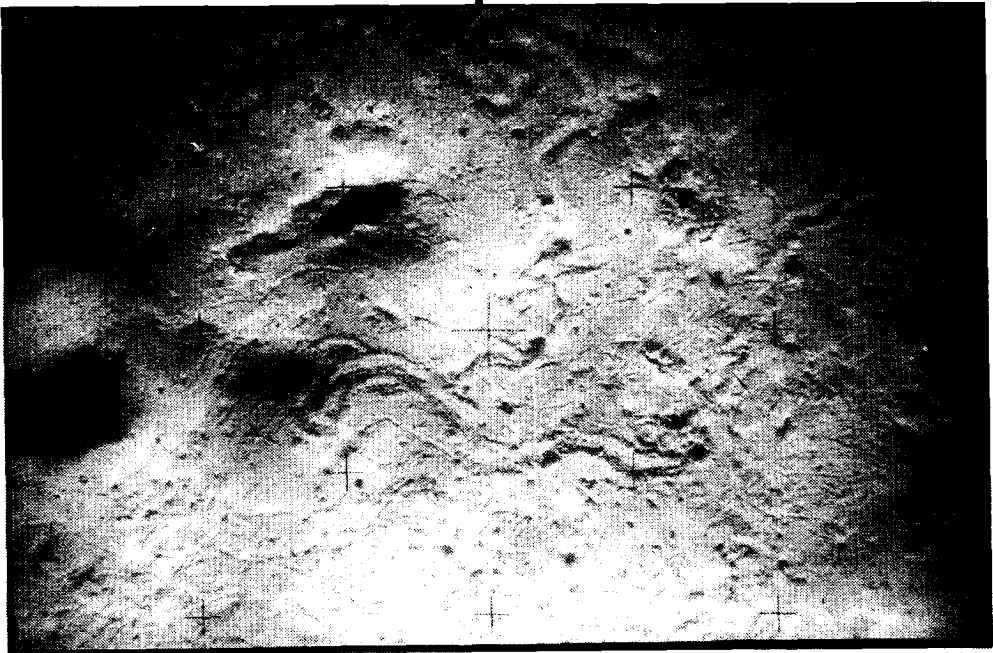
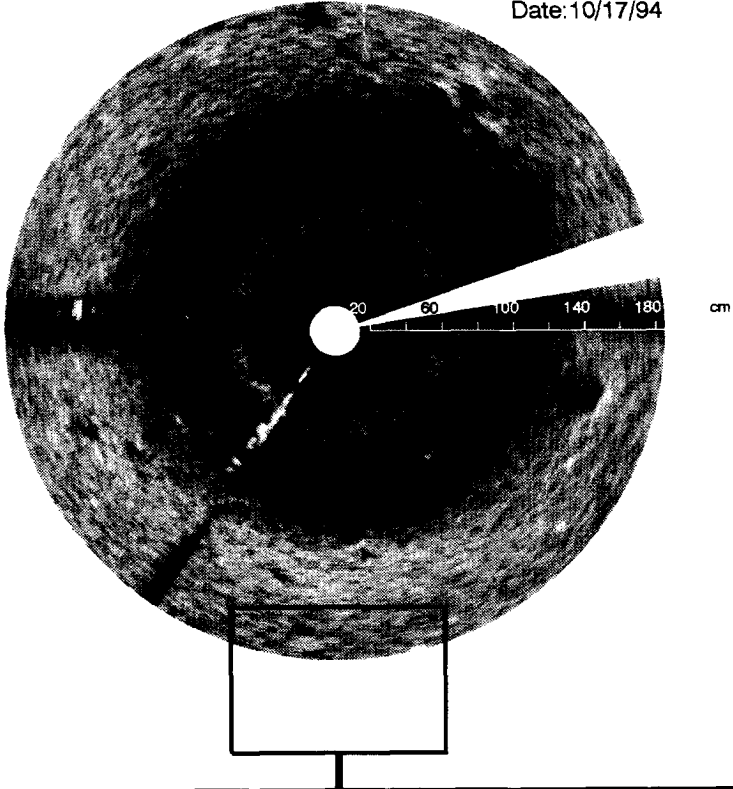
A comparison of the GGM estimate of  $\ell^{cw}$  and the acoustic point of highest slope change (Fig. 7) shows relatively good agreement between the model output and the data. The match, while not perfect, is good enough that it can be stated without ambiguity that the slope change point is measuring the top of the wave boundary layer. Error bars for the slope change estimate are best shown by the sensitivity to the “search parameter” in Fig. 7.

Above the wave boundary layer, a transition layer between it and the current boundary layer should be seen, perhaps of the form described in equation (9). Acoustic evidence for the transition layer comes from the observation that contributions to wave-induced turbulence above the GGM wave–current boundary layer are being seen. To show this, a slight diversion must be made to discuss an implication of the “tuned” acoustic response to the suspended sediment’s size. Firstly, the simple Rouse model sediment concentration profiles of equations (5) and (6) should be considered, whose (log–log) slopes are given by equation (8). Next, it is observed that for a system “tuned” to a certain narrow range of sizes, the fall velocity,  $w_n$ , which appears in the Rouse profile slope is approximately constant. Then, rewriting equation (8) as:

Fig. 5. Rotary sector scanning sonar image (top) and stereocamera image (bottom) of bottom microtopography at the STRESS C3 site. Top image shows areal density of burrows/mounds over a  $\approx 10 \text{ m}^2$  area with low feature resolution ( $0 \approx 1\text{--}10 \text{ cm}^2$ ). Bottom image shows high (photographic) resolution picture of a group of features near the bottom of the sonar image.

Sector Scanning Sonar Image (24 hour-image avg.)

Date: 10/17/94



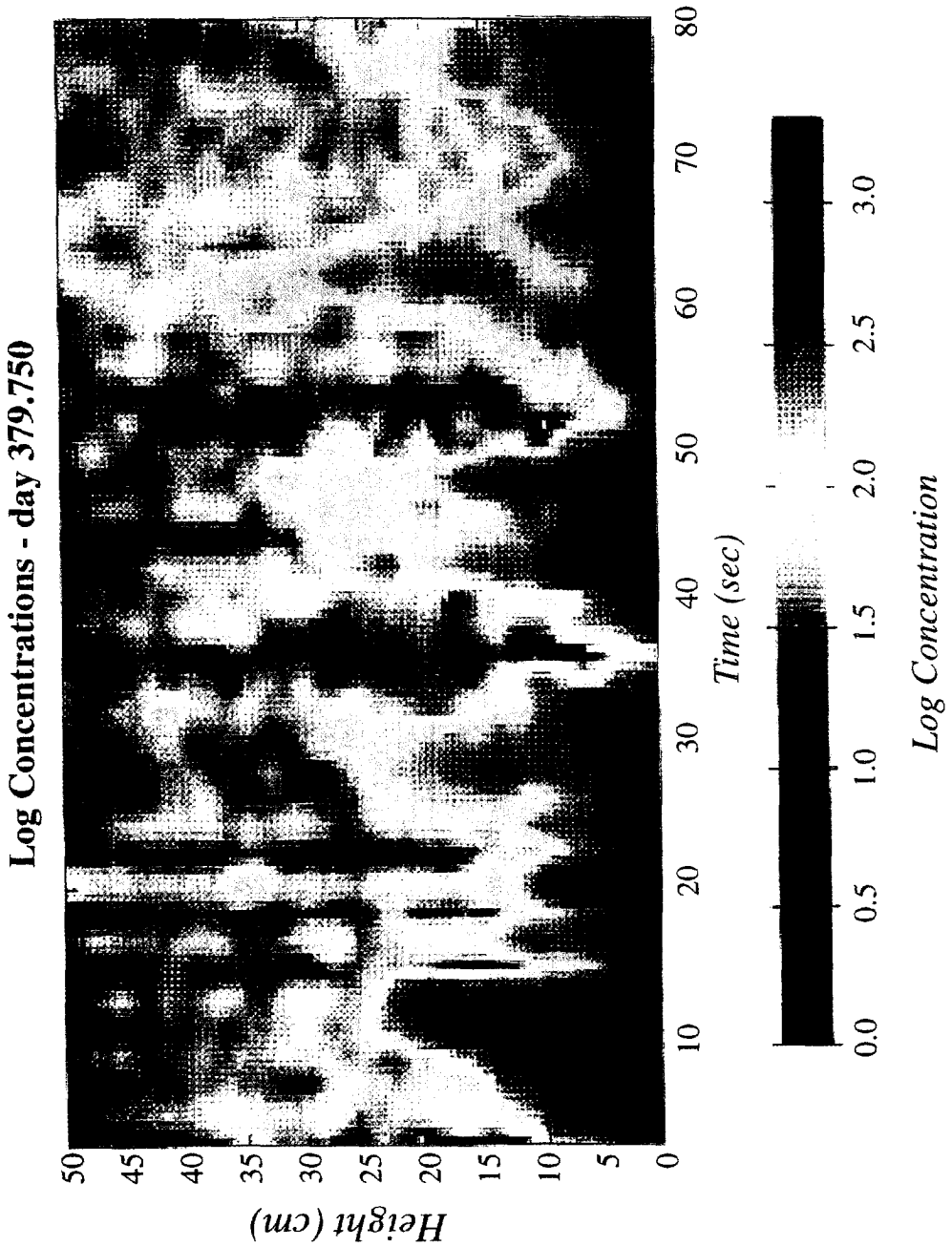


Fig. 11. Near-bottom plumes of sediment seen at the STRESS site at the initiation of a storm event. Above 30 cmab sediment is temporally homogeneous in nature; below, wave frequency oscillations are seen. Scale is  $\text{gms cm}^{-3}$ .

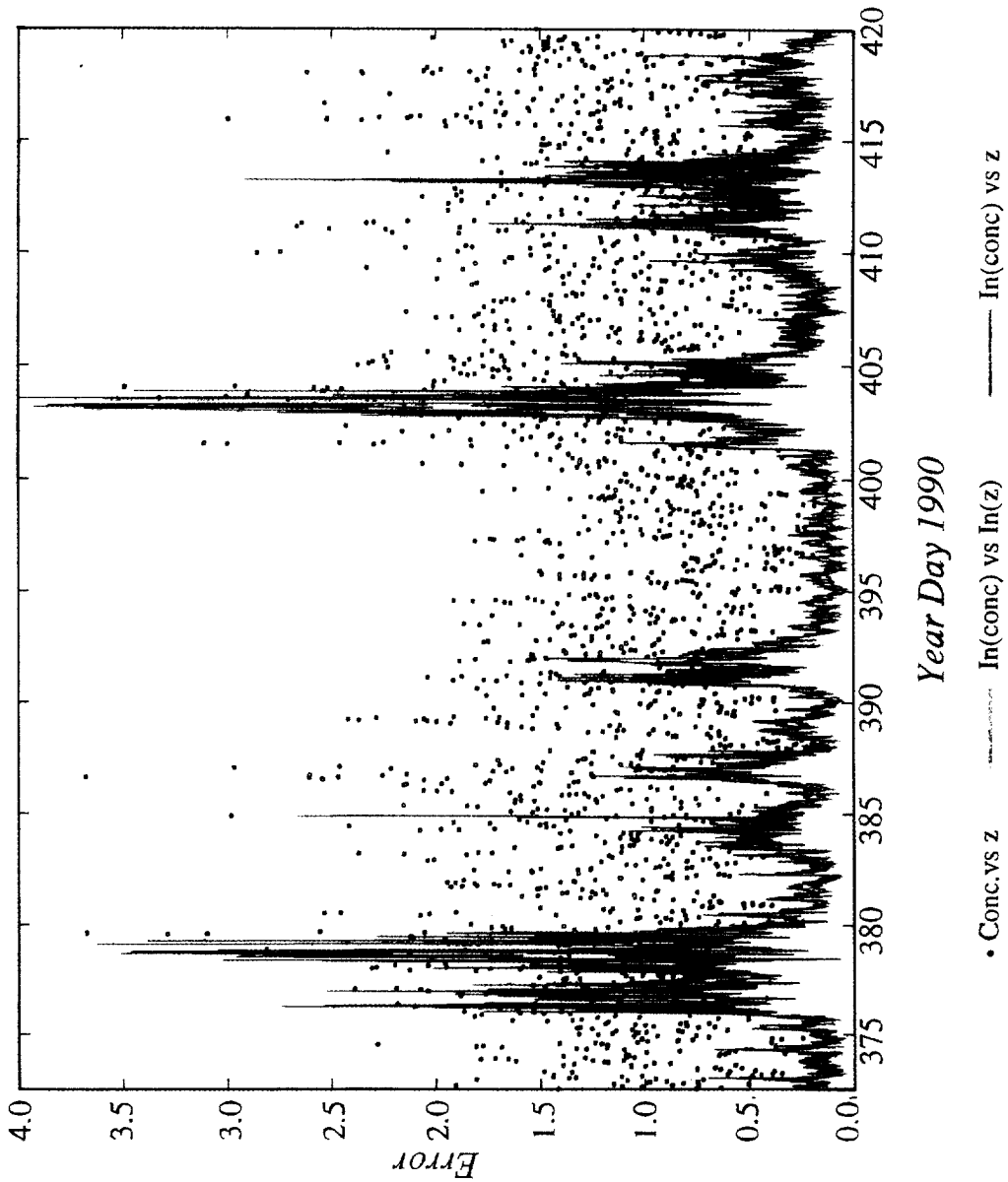


Fig. 14. Integrated error in  $\text{gms cm}^{-3}$  in fitting linear-linear, linear-log and log-log  $z$  vs  $C$  curves to the acoustic concentration profile data. The length of the profile fit was not normalized in order that the storm events would show more clearly.

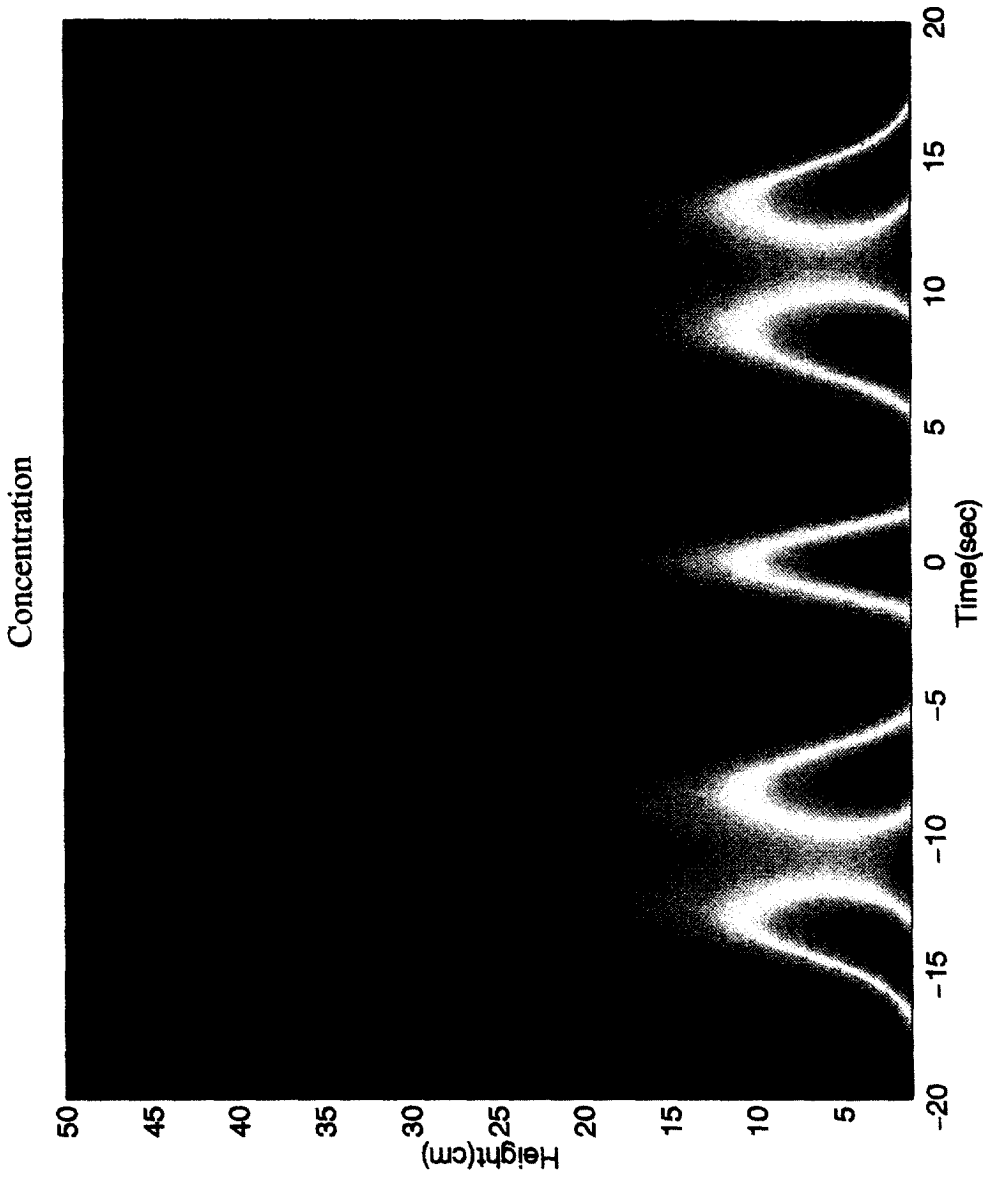


Fig. 15. Simple advective-diffusive model of the plume structure seen at the STRESS C3 site. "Hotter" colors denote higher concentration.

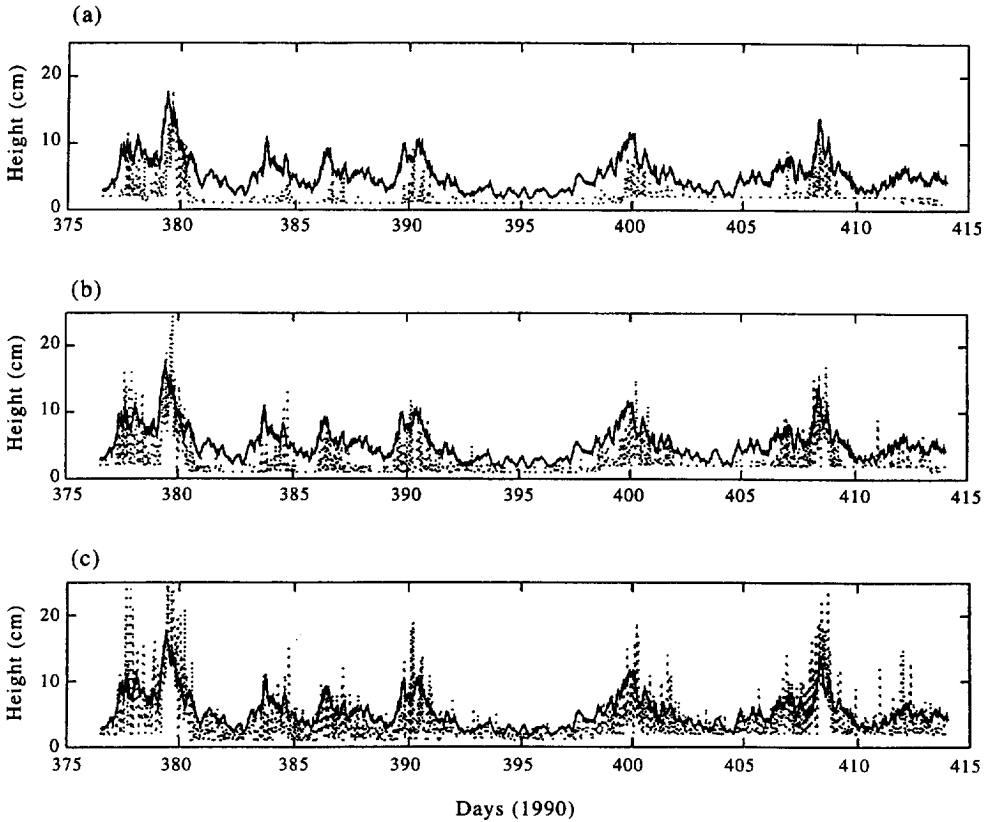


Fig. 7. Height of the wave boundary layer as produced by the GGM model (solid line) and as inferred by the lower “high-slope change” point in the acoustic backscatter data. Acoustic data are quantified into 1 cm range bins. Variation in the smoothing parameter used in searching for the maximum slope change point in the acoustic data leads to an effective error bar estimate of  $\delta$ , as seen for the three cases shown in (a), (b) and (c).

$$\begin{aligned}
 S^{-1} &= \left( \frac{\kappa}{w_n} \right) u_*^c & z > \delta_{cw} \\
 S^{-1} &= \left( \frac{\kappa}{w_n} \right) u_*^{cw} & z < \delta_{cw}
 \end{aligned} \tag{17}$$

it can be noted that the term in parentheses is now approximately constant and that the inverse of the slope above the GGM wave–current boundary layer is directly proportional to  $u_*^c$ , whereas the inverse of the slope within the GGM wave–current boundary layer is directly proportional to  $u_*^{cw}$ . Since  $\delta_{cw}$  has been measured directly from the abrupt slope change points in the data, the slopes above and below  $\ell^{cw}$  can be examined and compared to  $u_*^c$ ,  $u_*^{cw}$  and also  $u_b$  (the near-bottom wave velocity). If equations (3) and (4) correctly describe the eddy viscosity profile, a proportionality to  $u_*^c$  above  $\ell^{cw}$  should be seen. Dependence on  $u_*^{cw}$  and  $u_b$  above  $\ell^{cw}$  would imply that the older GM model needs modifications such as those seen in equation (9).

It is necessary first to look at the comparison of the acoustic slopes above  $\ell^{cw}$  to  $u_*^c$ ,  $u_*^{cw}$

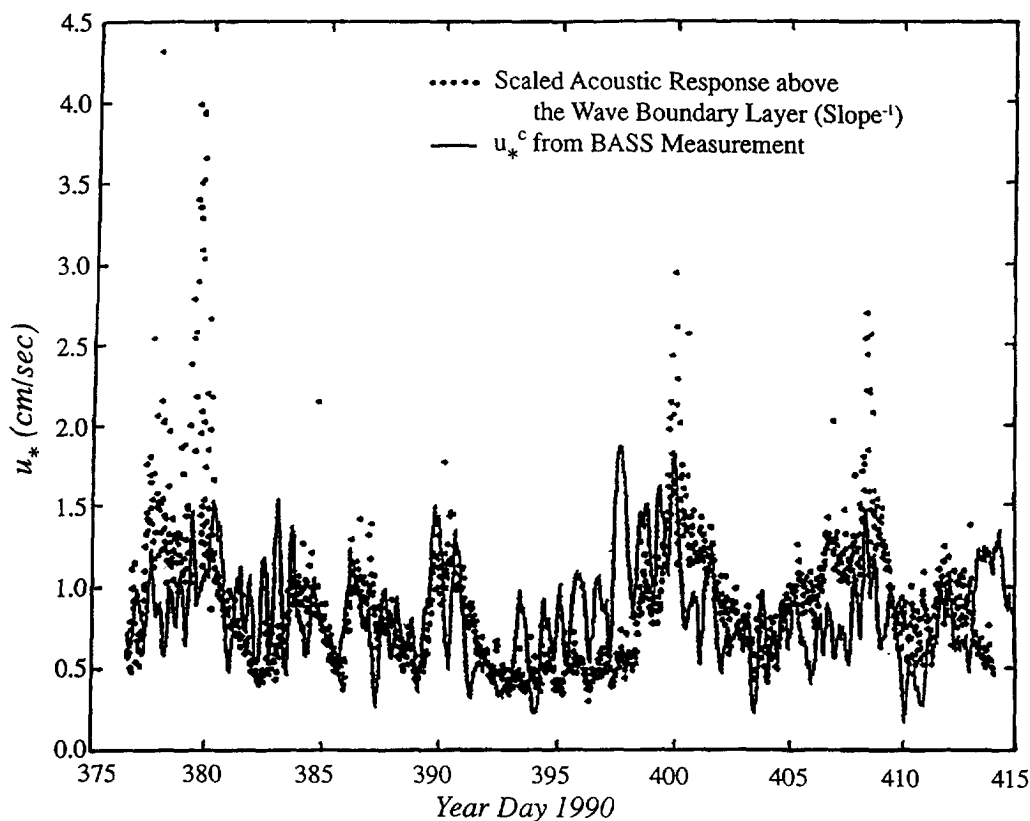


Fig. 8. Scaled inverse of acoustic concentration profile slopes above  $\delta$  vs  $u_*^c$ . Good agreement is seen except during storm events.

and  $u_b$ . Since the value of  $w_n$  is not precisely known, it is possible to allow a flexibility of scaling the inverse acoustic slopes to give a best fit to the above variables. (However, only one scale factor will be used to fit each time series!) In Fig. 8 a comparison of the scaled inverse acoustic slope measurement to  $u_*^c$  is shown, as obtained from the BASS measurement. It is seen that the comparison is not so bad, with the worst mismatch being to the “high energy” peaks in the acoustic data. In Fig. 9, the scaled acoustic slope comparison to  $u_b$ , the near bottom wave velocity, is shown. The large peak events are now a good fit, though at the loss of some of the good agreement during low energy periods. Finally, in Fig. 10 the scaled acoustic response is compared to  $u_*^{cw}$ . The overall agreement is now seen to be excellent, which implies: (1) that there are definitely wave and wave-current stress effects being seen above the older GGM model wave-current boundary-layer height,  $\ell^{cw}$ ; and (2) that a Rouse profile is not an unreasonable first guess at the transition layer profile shape. It is noted that using a Rouse profile is not consistent with the exponential shape of the intermediate layer profile indicated in equation (11). However, if the Rouse and exponential profiles are not too different in the transition region, as can be seen later, this simple approach makes sense, as it very clearly shows the wave and wave-current effects in that layer.

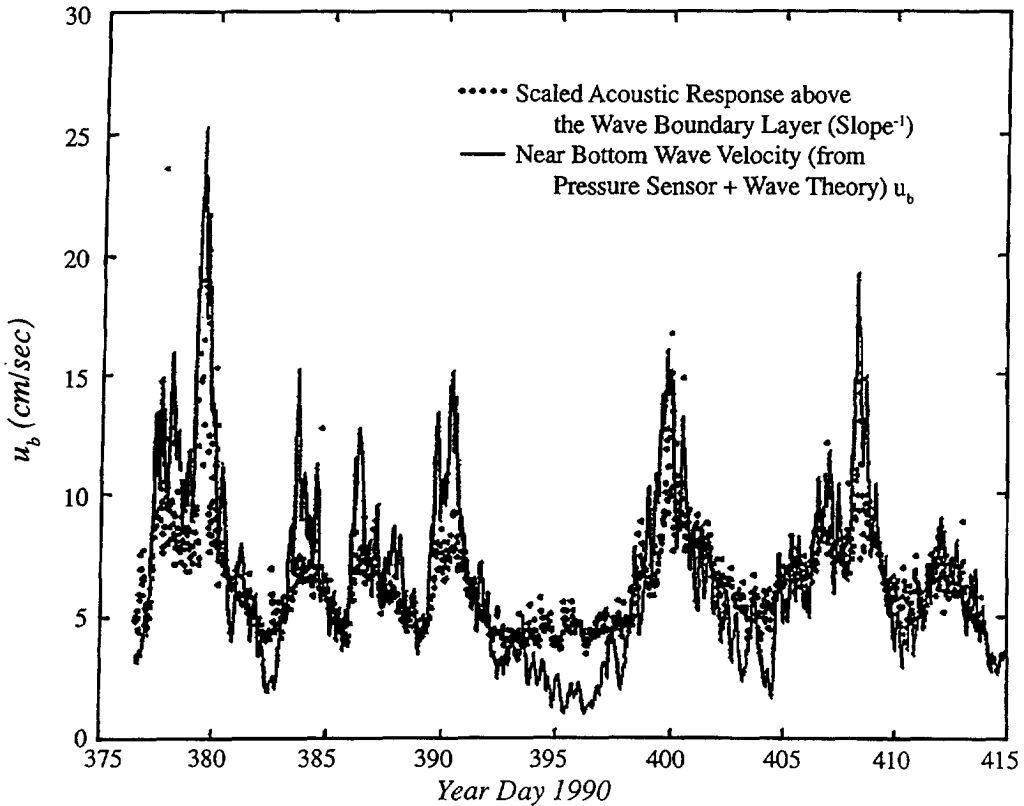


Fig. 9. Scaled inverse of acoustic concentration profiles slopes above  $\delta$  vs near-bottom wave velocity  $u_b$ . Larger events are seen to be due to wave stresses. However, some of the fit to lower energy periods (where currents are more effective) is lost.

As some measure of confirmation that the scaling approach used above is sensible, it is noted that in order for the scaled inverse acoustic slope curves and the  $u_*^c$  and  $u_*^{cw}$  curves to agree via equation (13),  $w_n$  must be approximately  $0.4 \text{ cm s}^{-1}$ . For a Stokes fall velocity law for a spherical particle of the density of quartz, this corresponds to about a  $60\text{--}80 \mu\text{m}$  diameter particle, which is reasonably close to the  $50 \mu\text{m}$  "tuning" assumed.

It is also noted that in examining the  $u_*^c$  and  $u_*^{cw}$  curves in Figs 8 and 10, tidal signals are clearly evident, particularly during periods of low wave activity. The inverse acoustic slope time series seem to show less tidal fluctuations, however, leading one to question the "higher frequency" (tidal frequencies and above) fit of the acoustic slopes to the  $u_*^c$  and  $u_*^{cw}$  data. However, the acoustic data, when spectrally analyzed, do show significant tidal energy. This is somewhat obscured by the noisiness of the acoustic slope time series. Also, sediment concentration is not as clean an indicator as currents of tidal motions, since advection, sediment patchiness and other effects can easily change the acoustic (inverse) slopes from the Rouse profile values.

Besides the evidence for an intermediate layer model from the slope change points and the slopes themselves, there is also the direct physical picture obtained from looking at the

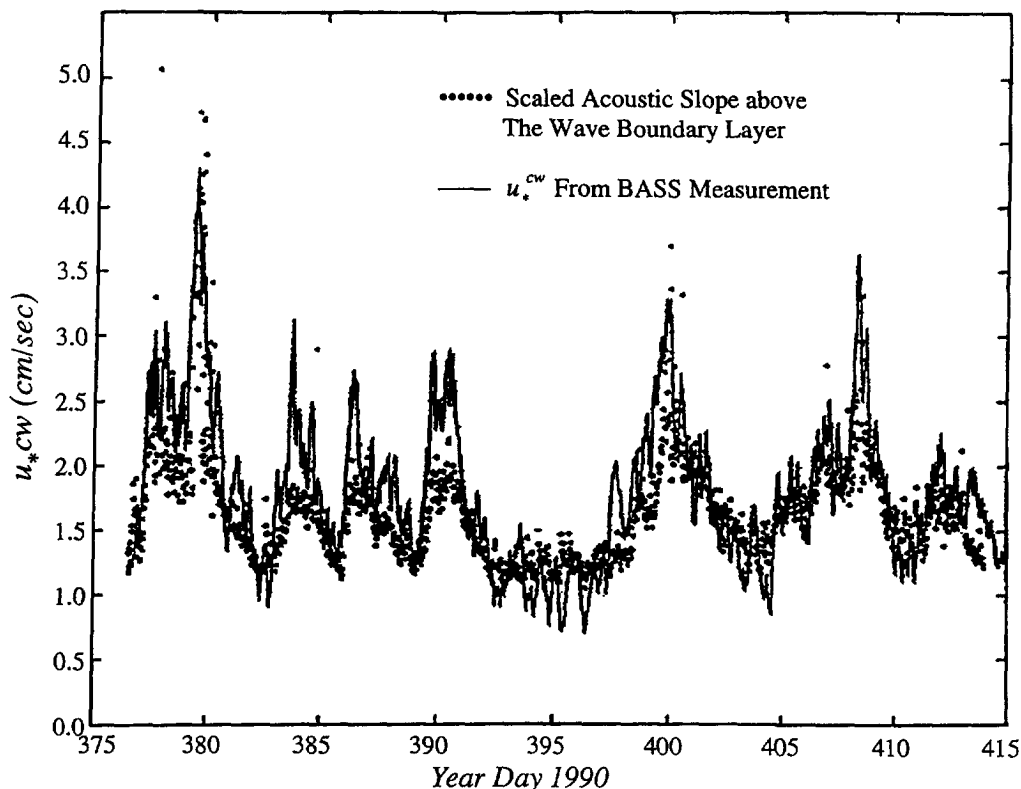


Fig. 10. Scaled inverse of acoustic concentration profile slopes above  $\delta$  vs  $u_*^{cw}$ . Good agreement is generally noted both in current and wave dominated regimes. The residual deviation is likely due, in most part, to deviation of the profile from the Rouse assumption made.

“fast sampled” ABSS measurements of concentration. Such a picture is shown in Fig. 11. In this picture, which was typical of a small benthic “storm” event at the STRESS site (i.e. a high energy period), one sees distinct plumes occurring at about 15-s intervals, which is the dominant surface gravity wave period at the site. The tops of these plumes rise to between 25 and 40 cmab, which is physically the top of the “transition layer” as measured by ABSS.

Interestingly, the tops of these plumes coincide reasonably well with the top of the transition layer in the extended GGM model at  $\ell^{\text{TRANS}} = \alpha\delta/\epsilon$ . This is shown in Fig. 12, which presents data for  $\ell^{\text{TRANS}}$  for which there was greater than a 5dB signal-to-noise ratio (SNR) for the acoustics, and thus the slope estimates can be trusted to some degree. This agreement may or may not be fortuitous, in that there is no apparent reason to see any connection between the top of an advected plume and a “transition point” as defined by a model of eddy viscosity that requires a continuity constraint on  $K(z)$ . In fact, one could perhaps use the top of the physical plumes to be a constraint on the form of the 1-D vertical eddy viscosity assumed, which might be a way to reduce 3-D effects to a 1-D form. Lower down in the boundary layer, from 0 to 10 cmab, one sees small, higher concentration pulses at twice the frequency of the larger plumes (this is particularly evident in the 40–80 s period

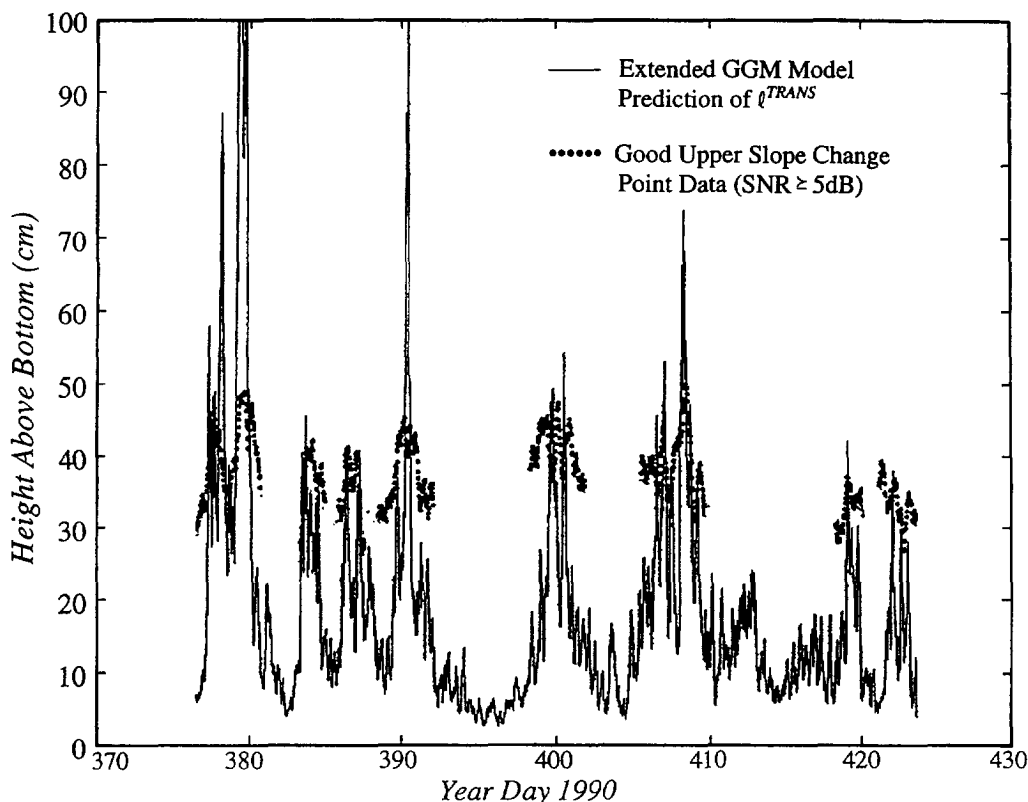


Fig. 12. Extended GGM model prediction of the height of the intermediate layer vs higher acoustic inflection point in ABSS data. Acoustic inflection point was considered trustworthy only for data with 5 db or above SNR. Good agreement is noted in about 70% of the events.

in Fig. 11). The top of these small plumes is the top of the GGM wave boundary layer. The plumes are not always as distinct as in Fig. 11 for all storm events; however, the top of the “transition layer” boundary still does remain distinct.

#### 4.1. Shape of the transition layer (exponential vs Rouse profile)

Having provided some evidence supportive of using a transition layer type of model, it is of interest to see if the acoustic profiles can also show some of the structure of the wave-current and current boundary layers as well. Figure 13 shows the  $\log C$  vs  $\log z$  slopes of the acoustic profile for the wave-current, transition and current boundary layer regions. These regions have been separated out by the change in concentration profile slopes which works well for the wave-current boundary-layer interface, but is only trustworthy for higher SNR periods in discriminating the higher interface. Looking at the wave boundary layer slope picture first [Fig. 13(a)], it can be seen that there is a rather odd looking, low frequency nature to the slope time series, which does not correlate to the storm events seen at the STRESS site. It is found that the slopes estimated in this rather thin region (0–10 acoustic range bins thick, typically) are adversely affected by the variations in the strength of the

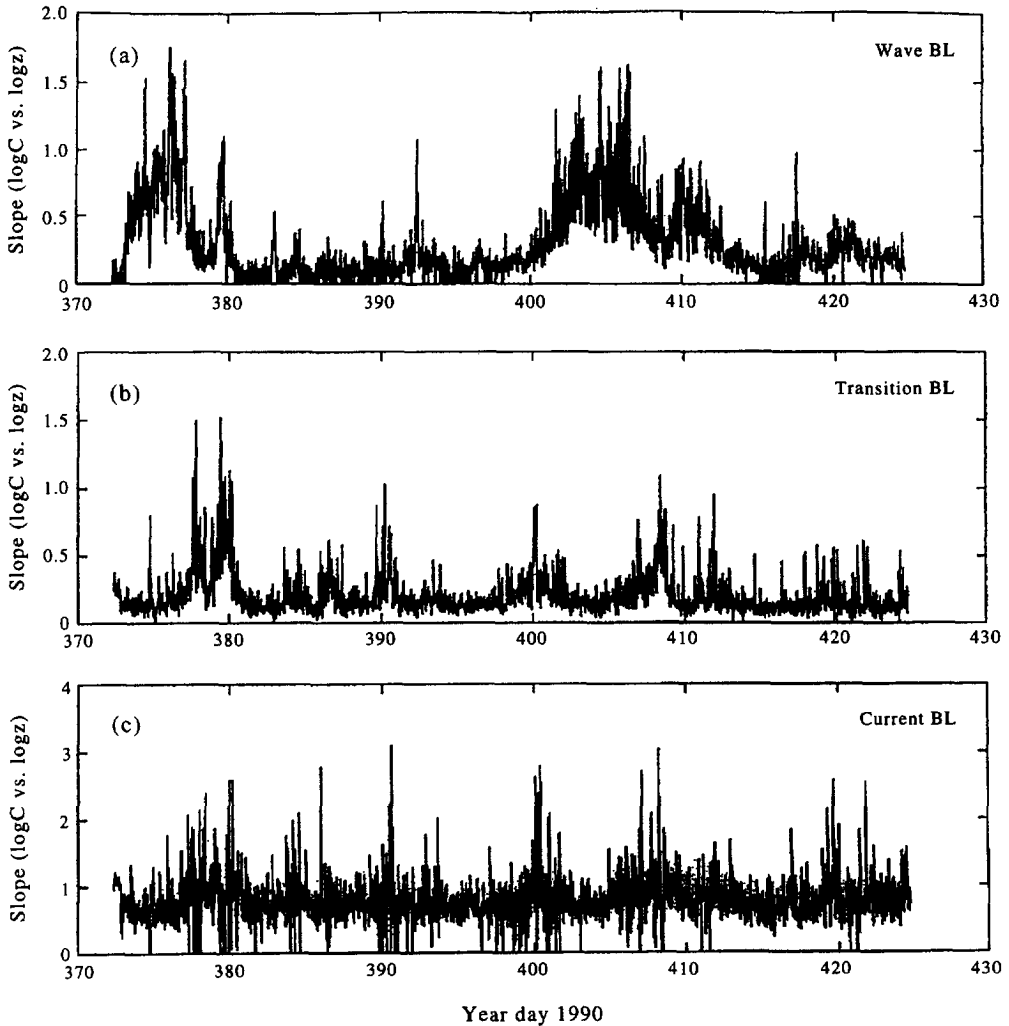


Fig. 13. (a) Slopes of acoustic data in the wave boundary layer. Paucity of data points and strong effects of near-bottom topography make these slopes unreliable. (b) Slopes of acoustic data in the "transition layer". (c) Slopes of acoustic data in the current boundary layer. Low SNR and paucity of data make these slopes unreliable.

bottom return. Even a slight angular change in the specular reflection off the bottom will change the echo strength significantly, and thus the estimate of the near bottom slope. Therefore, unfortunately, it can be seen that the wave boundary-layer profiles and slopes are not of high enough quality to infer  $u_*^{cw}$  from equation (13).

Looking at the current boundary layer [Fig. 13(c)], it is noted that the only time that this layer's slopes are trustworthy is when there is a good SNR, i.e. during storm events. However, during such events, the transition layer is thicker, leading to there being only a thin current boundary layer component measurable between  $\ell^{TRANS}$  and  $z = 50$  cmab. As a result, the 5 MHz ABSS measurement of this layer is also sub-par.

Turning to the shape of the transition layer [Fig. 13(b)], it is noted that the best fits of the acoustic data to a Rouse profile slope gave acceptable fits to the  $u_*^c$  and  $u_*^{cW}$  data in Figs 8 and 10. Thus, a Rouse profile is obviously not too inconsistent with the intermediate layer shape. However, somewhat better fits to the profile shape in that region were obtained using exponential profiles during storm events, as one would expect if equation (11) was more appropriate then. To see this it is necessary to look at the “integrated error” incurred in fitting linear–linear, linear–log, and log  $z$  vs log  $C$  curves to the acoustic profile data. This is shown in Fig. 14. It is quickly seen that linear–linear fit has the largest error, whereas the linear–log (red) and log–log (green) fits give much smaller, comparable errors. During storm events, the linear–log fit (exponential profile) gives the best fit — it is also during these events that the transition layer and advected plumes can be seen best. During low energy periods the log–log curve fits best; this is consistent with a (lower in height) current boundary layer dominating and having a Rouse profile. Thus, the profile shape fits are consistent with an extended GGM boundary layer eddy viscosity structure. It should be noted that the acoustic concentration profiles do have some irregularity associated with them, as well as calibration error, so that error bars need to be attached to the Fig. 14 result. The errors are rather hard to quantify for this particular figure, however, as each 80-s “average profile” realization has a large amount of random fluctuation error in it.

## 5. TEMPORAL 3-D SPATIAL STRUCTURE OF THE BOTTOM BOUNDARY LAYER

### 5.1. *Near-bottom plume structure*

The ABSS instrument measures a narrow beam width vertical profile of backscatter due to suspended sediments, which is ideal for studies of the 1-D structure of the BBL. It is also clear that 3-D effects are present in this vertical profile data. Consider, for instance, Fig. 11 which shows the plumes of sediment produced on day 379.750. In between plumes rising to 30–40 cmab, there are quite clear periods at 35, 53 and 70 s apparent in this data. This would imply that either: (1) sediments rose to  $\approx 35$  cmab and then fell out within  $\approx 7$ –8 s (this is the “instantaneously” 1-D model scenario); or (2) sediment plumes are being advected back and forth across the acoustic beam (the instantaneously 3-D model prediction). A fall of 35 cm in 7 s implies  $\approx 5$  cm s $^{-1}$  fall velocity, which is more appropriate to coarse sand than the  $\approx 50$   $\mu$ m particles that ABSS is seeing at the STRESS site. Thus, it is apparent that instantaneous 3-D BBL effects are being seen.

One also notices that above the plumes, the concentration profile looks more or less homogeneous. At this point, which the authors conjecture is the lower edge of the current boundary layer, a simple 1-D model might be appropriate even on an instantaneous basis, as the clouds of suspended sediment have seemingly “coalesced” horizontally, as opposed to the near bottom plumes which maintain their identity in the wave and transition boundary layers. Thus, it is hypothesized that an instantaneously 3-D boundary layer up to the top of the plumes and a more “time-independent” 1-D homogeneous layer above are being observed. This is quite consistent with the “advective–diffusive” model (Nielsen, 1992), in which the larger particles, to which ABSS is more sensitive, form the advected plumes, whereas the finer particles form the diffusive component seen above the plumes. With time averaging over a suitable number of wave periods, the entire boundary layer can perhaps be treated as 1-D, which is the more standard usage of “1-D BBL models”. The plume

structure seems to be most evident at or near storm peaks, when one would expect to see larger particles transported near the bottom. At other times, one still sees some of the “spotted carpet” effect of horizontal advection of local inhomogeneity, but nothing like the distinctive “storm plumes”.

### 5.2. *Measurements of bottom microtopography by sector scanning sonar and stereocamera*

As mentioned, our thinking about 1-D vs 3-D structure in the near bottom boundary layer was affected strongly by the large scale biogenic roughness seen in the 1994–1995 data set. This section briefly discusses the physical properties of this roughness and the authors also conjecture why it was not seen in the 1990–1991 stereocamera data (e.g. Wheatcroft, 1994).

The biological mounds/burrows which were clearly seen in the 1994–1995 sector scanner and contact camera surveys had durations of weeks to months. Created by either small crustaceans or fish (both of which were seen in R. Wheatcroft’s stereocamera photos of the mounds), these features are moderately eroded by “typical” transport events and are only washed away by the largest storm events. Moreover, eroded burrows/mounds are maintained and new ones are occasionally created. Thus, these features create a 3-D roughness field over at least the fall and winter months (which were observed) and perhaps longer. The mounds/burrows are of rough order 10 cm across, 3 cm high and 10 cm deep, and are found in small groups of one to five holes, each in the order of 10 cm apart. Spacing between groups is in the order of 1 m apart and it is this scale that the authors conjecture is the source of the 3-D effects. Moreover, if the 12–14 mounds seen in the 10 m<sup>2</sup> field of view are taken to have a cylindrical volume of  $\pi r^2 h = 785 \text{ cm}^3$  each available for transport, this gives a value of 942 cm<sup>3</sup> m<sup>-2</sup> available — a fairly significant amount. (Equivalently, this corresponds to eroding the entire bottom by 0.1 cm in depth).

It should be noted that such burrows were not seen in Wheatcroft’s time lapse images during the 1990–1991 deployment. This might have been due to the smaller field of view of the stereocamera (0.8 m<sup>2</sup>) compared to the sector scanner (10 m<sup>2</sup>). In that the field of view of the camera was less than the mean spacing between (clusters of) mounds, it would not be totally surprising if the mounds were missed. However, it is also possible that the mounds were not present at all during the 1990–1991 deployment, in which case other mechanisms for the 3-D effects observed need to be identified. This latter possibility seems less likely, however, in light of a previous study by Cacchione *et al.* (1983) using box cores and time-lapse photography at the C3 STRESS site. This study also found copious mounds and burrows, similar to those observed in the present study. (Unfortunately, the study by Cacchione *et al.* was not useful for producing an areal density estimate to compare to the one generated in the present study.)

### 5.3. *Plume advection model*

Given the plume structure seen in the ABSS acoustic data and the possible existence of “point sources” of sediment plumes (the mounds), it would make sense to look at “frozen turbulence” advection of a sediment plume kicked up at such a site by the local waves and currents. This model is presented to demonstrate that several “unexpected” features of the ABSS data (Fig. 11) may be explained by a simple 3-D structure. These features include the  $2f_{wave}$  peaks seen near the bed which coalesce into  $f_{wave}$  peaks above  $\delta_{cw}$  and the large

variability in vertical structure away from the simple Rouse profile on time scales of a wave period. These attributes are explained below by an isolated plume of sediment advected by the combined velocity field of a logarithmic mean profile and uniform wave motion.

Suppose a plume is produced at a localized spot, such as one of the mounds, at time  $t = 0$ ; then in a 2-D ( $x, z$ ) model, the plume is advected by a velocity field given by:

$$U(z, t) = \frac{u_*^c}{\kappa} \ln\left(\frac{z}{z_0}\right) + U_w \cos(\omega t), \quad (14)$$

where  $U_w$  is the wave velocity amplitude and  $\omega$  is the wave angular frequency. The particles are displaced by an amount:

$$X(z, t) = \frac{tu_*^c}{\kappa} \ln\left(\frac{z}{z_0}\right) + \frac{U_w}{\omega} \sin(\omega, t) + X(z, 0). \quad (15)$$

Now an initial plume with a concentration profile:

$$C(x, z) = C(z_{ref}) \exp(-x^2/\Delta^2) - \left(\frac{z}{z_{ref}}\right)^{-w_n/\kappa u_*^c} \quad (16)$$

is assumed, where  $\Delta$  is the plume width to be specified. Thus, the ABSS, which, due to its narrow beam width, acts as a vertical 1-D sensing array, will observe a time series of vertical concentration profiles given by:

$$C(t, z) = C(z_{ref}) \exp(-X^2(z, t)/\Delta^2) \left(\frac{z}{z_{ref}}\right)^{-w_n/\kappa u_*^c}. \quad (17)$$

Using the above equations in a simple MATLAB computer code with parameters representative of the STRESS site produces plume structures as seen in Fig. 15. One immediately notices that this model reproduces both the  $2f_w$  structures seen in the wave boundary layer and the  $1f_w$  plume structure extending further up (where  $f_w$  is the dominant wave frequency). It is noted that both wave and current advection are needed to obtain this structure, i.e. either one alone does not suffice. This model also assumes that the wave, current and source-receiver vectors are all in a common plane, which is probably not true of the field data most of the time. Thus, the 2-D planar model probably predicts a somewhat simpler plume structure than that observed in the field. However, the fact that the plume structure is basically reproduced is some grounds to think that the model is not too far afield. The time average of the plumes in Fig. 15 yields an exponentially decaying profile in height, in agreement with that observed during storm events (Fig. 14).

## 6. DISCUSSION AND CONCLUSIONS

This paper has attempted to describe the nature of the lower 50 cm of the bottom boundary layer at the STRESS site by looking at 5 MHz acoustic backscatter profiles obtained during the winter 1990–1991 deployment. The wave boundary layer was rather clearly defined in the sediment concentration vertical profiles which the acoustics measured. Above the wave boundary layer, the acoustics showed “plumes” of sediment which are clearly advected in three dimensions. Rotary sector scanning sonar, stereocamera and survey camera images from the 1994–1995 STRESS deployment showed distinct biogenic

roughness elements which the authors hypothesize might be causing the 3-D plumes seen in the 1990–1991 acoustic backscatter data.

Should the authors' conjecture of significant 3-D advection by the biogenic roughness elements prove correct, it would raise three (rather closely related) questions: (1) what is the difference in the transport, both mean and fluctuating, between the STRESS site with biogenic mounds and 3-D plumes present, and the previous and still prevalent 1-D view of the site? (2) can one still use simple 1-D diffusive models with suitably modified vertical eddy viscosity profiles to account for 3-D effects? and (3) the concept of critical erosion stress appears to need modification since presumably the wave current is spatially uniform and yet erosion is occurring with great spatial non-uniformity. Rather, one is left with the image of sediments located near burrows and mounds subject to non-uniform stress which exceeds critical erosion conditions. Thus, sediment is locally put into suspension before the "average" wave and current stress exceeds critical stress sufficient to erode sediments.

This paper has argued that some 3-D effects are indeed present and that they are possibly due to biogenic features seen in 1994–1995. However, lacking conclusive evidence that the mounds contributed to the 3-D roughness in 1990–1991, it would be premature to model the differences between the 1-D and 3-D cases. It is the authors' hope that the 1994–1995 STRESS data will eventually allow a better answer to this question to be obtained. As to whether one can use 1-D models to account for 3-D effects, the data seem to indicate that this may be possible. However, the exact conditions under which one may do this need to be specified by some mathematical work and better data, not by the (possibly coincidental) agreement of the present field data plume heights with the top of the transition layer.

*Acknowledgements*—First and foremost, the authors would like to thank Dr Joseph Kravitz of the Office of Naval Research (ONR) for his support of the STRESS program scientifically, financially and personally. Joe's faith in STRESS's goals and personnel was the main factor in making that program, of which the above work represents only a small fraction, possible and (the authors feel) successful. All the authors were funded under ONR code 1125GG (now 325GG) for this work. Experimental debts are many. The authors thank Dr Sandy Williams for making his BASS current meter data and analyses available and Dr Rob Wheatcroft for use of his camera data. In deploying the equipment John Kemp, John Bouthillette, the numerous other STRESS investigators, and the crews of the R.V. *Wecoma* and R.V. *Point Sur* are to be thanked. Kudos go to Paul Boutin and Deep Ocean Engineering for recovering the ABSS tripod after its release had failed. Nick ("Jean Luc") Witzell was the project engineer for the ABSS, ably taking over for Rick Filyo whose tragic death soon after the initial deployment of ABSS saddened us all. The authors thank Drs Ole Madsen of MIT, Alex Hay of Memorial University, and Drs John Trowbridge and Rob Wheatcroft of WHOI for their valuable discussions and comments. The programming assistance of Ms Janet Fredericks and typing by Ms Bonnie Gouzas is also gratefully acknowledged. This paper is WHOI contribution number 8810.

## REFERENCES

- Cacchione, D. A., Drake, D. E., Grant, W. D., Williams III, A. J. and Tate, G. B. (1983) *Variability of Sea-floor Roughness Within the Coastal Ocean Dynamics (Code) Region*. Woods Hole Oceanographic Institution Technical Report WHOI-83-25.
- Fredsoe, J. and Deigaard, R. (1992) *Mechanics of Coastal Sediment Transport*. World Scientific Press, Singapore, 369 pp.
- Glenn, S. M. and Grant, W. D. (1987) A suspended sediment stratification correction for combined wave and current flows. *Journal of Geophysical Research* **92**, 8244–8264.
- Grant, W. D. and Madsen, O. S. (1979) Combined wave and current interaction with rough bottom. *Journal of Geophysical Research* **84**, 1797–1808.
- Grant, W. D. and Madsen, O. S. (1986) The continental shelf bottom boundary layer. *Annual Review of Fluid Mechanics* **18**, 265–305.

- Hay, A. E. (1983) On the remote acoustic detection of suspended sediments at long wavelengths. *Journal of Geophysical Research* **88**, 7525–7542.
- Hay, A. E. and Wilson, D. J. (1994) Rotary sidescan images of nearshore bedform evolution during a storm. *Marine Geology* **119**, 57–65.
- Lentz, S. J. and Trowbridge, J. A. (1991) The bottom boundary layer over the California Shelf. *Journal of Physical Oceanography* **21**, 1186–1201.
- Lynch, J. F. (1985) Theoretical analysis of ABSS data for HEBBLE. *Marine Geology* **66**, 277–289.
- Lynch, J. F., Irish, J. D., Sherwood, C. R. and Agrawal, Y. C. (1994) Determining suspended particle size information from acoustical and optical backscatter measurements. *Continental Shelf Research* **14**(10–11), 1139–1165.
- Madsen O. S. and Wikramanayake, P. N. (1991) *Simple Models for Turbulent Wave–Current Bottom Boundary Layer Flow*. Dredging Research Program Report DRP-91-1.
- Nielsen, P. (1992) *Coastal Bottom Boundary Layers and Sediment Transport*. World Scientific Press, Singapore, 324 pp.
- Rouse, H. (1937) Modern conceptions of the mechanics of fluid turbulence. *Transactions of the American Society of Civil Engineers* **102**, 463–554.
- Sherwood, C. R., Butman, B., Cacchione, D. A., Drake, R. E., Gross, T. F., Sternberg, R. W., Wiberg, P. L. and Williams, A. J. (1994) Sediment transport events on the northern California continental shelf during the 1990–1991 STRESS experiment. *Continental Shelf Research* **14**(10–11), 1063–1099.
- Trowbridge, J. H. and Lentz, S. J. (1991) Asymmetric behavior of an oceanic boundary layer above a sloping bottom. *Journal of Physical Oceanography* **21**, 1171–1185.
- Trowbridge, J. H. and Nowell, A. R. M. (1994) An introduction to the sediment transport on shelves and slopes (STRESS) program. *Continental Shelf Research* **14**(10–11), 1057–1061.
- Wheatcroft, R. (1994) Temporal variation in bed configuration and one-dimensional bottom roughness at the mid-shelf STRESS site. *Continental Shelf Research* **14**(10–11), 1167–1189.
- Wheatcroft, R. A. and Butman, C. A. (1997) Spatial and temporal variability in aggregated grain-size distributions, with implications for sediment dynamics. *Continental Shelf Research* **17**, 367–390.
- Williams, A. J., Tochko, J. S., Koehler, R. L., Grant, W. P., Gross, T. F. and Dunn, C. V. R. (1987) Measurement of turbulence in the ocean bottom boundary layer with an acoustic current meter array. *Journal of Atmospheric and Oceanic Technology* **4**, 312–327.